2018 IEEE Conference on Control Technology and Applications (CCTA)
Copenhagen, Denmark, August 21-24, 2018

Fuel Efficient Moving Target Tracking using POMDP with Limited FOV Sensor

Christopher M. Eaton[1], Lucas W. Krakow[2], Edwin K.P. Chong[2] and Anthony A. Maciejewski[2]

Abstract— **The ability to effectively track moving targets is a critical capability for future autonomous aircraft. While many methods have been developed for performing target tracking, minimal work has focused on fuel-efficient options to extend mission duration. The ability to tightly track a target is critical for certain missions; however, increased tracking errors can be accepted in certain scenarios to extend endurance. Partially Observable Markov Decision Processes (POMDPs) have been shown to be effective for tracking fixed and moving targets. This paper provides a fuel-efficient option that shows a 10% endurance increase with adequate target tracking. The algorithm provides tracking with a limited field of view fixed sensor that will have limited observations depending on mission requirements. The POMDP formulation proposed in this paper is robust enough to handle observations while also providing options for improved fuel efficiency. We perform 500 Monte Carlo simulations per configuration to provide statistical confidence in the performance of the algorithm.**

I. INTRODUCTION

Unmanned aerial vehicles (UAVs) are well suited for performing dull, dirty, and dangerous missions normally performed by manned aircraft. One mission of critical interest is tracking moving targets. Significant research has been performed in numerous UAV control areas including path planning for target tracking [1]. However, the majority of path planning algorithms developed to date are focused on completing a specific mission task with a focus on tracking accuracy, target coverage, or expediency of mission completion. This approach provides satisfactory performance but generally result in less than desired UAV dynamics and limited endurance. There is limited consideration for fuel efficiency of the vehicle in the decision process of most of the algorithms. Ignoring the fuel efficiency concern can result in shorter missions or limit the mission effectiveness.

Previously, we had presented a robust path planning algorithm for a limited field of view sensor utilizing a partially observable Markov decision process (POMDP) with a nominal belief-state optimization (NBO) approximation [2], [3], [6]. These efforts have shown the ability of POMDP with NBO to perform effective path planning for tracking fixed and moving targets with a limited field of view (FOV) sensor. Additionally, collision avoidance and wind compensation schemes were also shown to be effective using the same POMDP algorithms [4]. The POMDP with NBO approach uses a receding horizon method that is computationally efficient and provides effective responses to changes in target dynamics or environmental changes. This method also provided a robust capability for tracking the targets across a range of altitudes and sensor configurations.

Here, we design a UAV control method that uses POMDPs with NBO approximation for a fixed FOV sensor with fuel efficiency considerations. We build upon our previous efforts [2], [3], [4], [5], that have shown the POMDP provides sufficient path planning for a UAV tracking of ground based fixed or moving targets. The cost function is modified to add in variable fuel burn considerations to improve mission endurance. The performance is evaluated using the tracking errors and the fuel burned during the simulations for multiple fuel burn options. The contribution of this paper is to show that the POMDP with NBO can provide effective target tracking while improving fuel efficiency. In this paper, we focus on non-evasive moving targets with limited observations.

This paper is organized as follows. Section II provides the problem statement. The development of the POMDP and NBO approximation is provided in Section III. Section IV discussed the UAV kinematics and sensor calculations. A fuel burn cost function is developed in Section V and a weighted trace penalty is discussed in Section VI. In Section VII, the experiments and results of the updated algorithm are presented. Conclusions are provided in Section VIII.

II. PROBLEM SPECIFICATION

Ground targets moving in 2-D at constant speed will be tracked. A simplified UAV motion model with forward acceleration and bank angle controls is used. The UAV has a limited speed range that is controlled by commanding longitudinal acceleration. The UAV bank angle is used to change UAV heading, while also changing the sensor observation area. A fixed FOV sensor mounted on the bottom of the vehicle provides a limited observation measurement of target location. Spatially varying random errors, based on UAV and target locations, corrupt the accuracy of the target location measurements. The fuel burn of the UAV is calculated based on the speed and bank angle of the UAV. The UAV altitude can be set for a given scenario, but will maintain a constant altitude during that entire scenario. Changing the UAV altitude is effectively the same as changing the sensor size or FOV. The objective is to provide a spectrum of options

[1]Christopher M. Eaton is with the department of Systems Engineering student at Colorado State University, Fort Collins, CO 80523 eatonc@rams.colostate.edu

[2]Lucas W. Krakow, Edwin K. P. Chong, and Anthony A. Maciejewski are with the Electrical & Computer Engineering Department, Colorado State University, Fort Collins, CO 80523 lucas.krakow, Edwin.Chong@colostate.edu, aam@colostate.edu

Supported in part by NSF grant CCF-1422658 and by the CSU Information Science and Technology Center (ISTeC).

to balance the minimization of the mean-squared tracking error with the fuel efficiency of the UAV.

III. POMDP AND NBO APPROXIMATION

A POMDP is a discrete time controlled dynamical process that is useful for modeling resource control problems. A POMDP, unlike a Markov Decision Process that has perfect knowledge of the system state, has some state information that is not directly observed. The NBO approximation method has been shown as computationally efficient for guidance optimization. The method described here builds on our earlier papers [2], [3], [4], [5], [6].

A. POMDP Ingredients

States: The POMDP states represent time evolving system features. Three subsystems are defined: the sensors, the targets, and the tracker. At time k, the state is defined as $x_k = (s_k, \chi_k, \xi_k, \mathbf{P}_k)$, where s_k is the state of the sensor, χ_k is the target state, and $(\xi_k, \mathbf{P}_k)$ is the tracker state. The sensor state is the UAV position and velocities, and the target state is the target position, velocities, and accelerations. The tracker state is a posterior mean vector, ξ_k, and posterior covariance matrix, $\mathbf{P}_k$, of a standard Kalman filter [7], [8].

Actions: The actions for this problem, or the available system controls, are UAV forward acceleration and the bank angle. Specifically, at time k the forward acceleration, a_k, and bank angle, ϕ_k, define actions $u_k = (a_k, \phi_k)$ of the UAV.

Observations and Observation Law: The target states are not fully observable; at any given time a random observation of the target state may be available. Let χ_k^{pos} be the target position vector and s_k^{pos} be the sensor/UAV position vector. The observation of the target's position can be expressed by:

$$z_k^{\chi} = \begin{cases} \chi_k^{pos} + w_k, & \text{if target is visible} \\ \text{no measurement}, & \text{otherwise} \end{cases} \quad (1)$$

where the random measurement error, w_k, has a distribution dependent on target and UAV locations. Full observability is assumed for Sensor/UAV and tracker states.

State-Transition Law: The state-transition law defines the next-state distribution of the three predefined subsystems given a current state and action pair of each subsystem. The sensor state evolves by $s_{k+1} = \Psi(s_k, u_k)$, where Ψ is a mapping function (defined later). The target state progresses according to $\chi_{k+1} = f(\chi_k) + \nu_k$, with independent and identically distributed random noise sequence, ν_k, and a target motion model, f (also defined later). Kalman filter equations with joint probabilistic data association (JPDA) provide tracker state evolution [7], [9]. The update equation is only evaluated when target observations are available, otherwise only the prediction step in the Kalman filter is performed.

Cost Function: Our cost function, which is the action cost for a given state, considers the mean-squared error between the tracks and the targets: $C(x_k, u_k) = E_{\nu_k, w_{k+1}}[\|\chi_{k+1} - \xi_{k+1}\|^2 | x_k, u_k]$

Belief State: The underlying state posterior distribution, updated incrementally via Bayes rule with observations, defines the belief state. At time k, the belief state is $b_k = (b_k^s, b_k^{\chi}, b_k^{\xi}, b_k^{\mathbf{P}})$, where $b_k^s = \delta(s - s_k)$, $b_k^{\xi} = \delta(\xi - \xi_k)$, $b_k^{\mathbf{P}} = \delta(\mathbf{P} - \mathbf{P}_k)$ (because of full tracker and sensor state observability), and b_k^{χ} is the posterior distribution of the target state.

B. Optimal Policy

The objective is to choose actions that minimize the expected cumulative cost over a time horizon $H, k = 0, 1, ..., H-1$. For a time horizon H, the expected cumulative cost can be written as $J_H = E[\sum_{k=0}^{H-1} C(x_k, u_k)]$. Historical knowledge of all observable quantities up to time $k-1$ should inform the chosen action at time k. If an optimal choice of actions exists, then there exists an optimal action sequence that depends only on "belief-state feedback" [10]. Therefore, the belief states can be used to write the objective function as: $J_H = E[\sum_{k=0}^{H-1} c(b_k, u_k) | b_0]$, where $c(b_k, u_k) = \int C(x, u_k) b_k(x) dx$.

Bellman's principle of optimality [11] provides for the optimal objective function value J_H^* given the current belief state b_0. The optimal objective function can be written as: $J_H^*(b_0) = \min_u \{c(b_0, u) + E[J_{H-1}^*(b_1) | b_0, u]\}$, where b_1 is the random next belief state, J_{H-1}^* is the optimal cumulative cost over the horizon $H-1, k = 1, 2, ..., H-1$, and $E[\cdot | b_0, u]$ is the conditional expectation given the current belief state b_0 and an action u taken at time $k = 0$. Given the current belief state b_0, the Q-value of taking an action u is defined by $Q_H(b_0, u) = c(b_0, u) + E[J_{H-1}^*(b_1) | b_0, u]$. At time $k = 0$ the optimal policy, from Bellman's principle, can be written as $\pi_0^*(b_0) = \text{argmin}_u Q_H(b_0, u)$. The optimal policy at time k is $\pi_k^*(b_k) = \text{argmin}_u Q_{H-k}(b_k, u)$.

The second Q-function term is difficult to obtain exactly. Studies of numerous methods to approximate the Q-values have been performed [5], [12], [13], [14], [15], [16], [17], [18]. The NBO approximation method, introduced in [5] along with other guidance problem approximations and techniques, is used here.

C. NBO Approximation

Although a few approximation methods to solve POMDPs are available, we chose the NBO method because of low computationally cost relative to other POMDP approximation methods like foresight optimization, hindsight optimization, policy rollout, and Q-learning [10]. In practice, real-time implementation of a UAV guidance algorithm requires a method that is not computationally prohibitive. Our previous work [3], [2] showed acceptable computation efficiency for the NBO algorithm.

Given N_{targs} targets, the target state is represented as $\chi_k = (\chi_k^1, \chi_k^2, ..., \chi_k^{N_{\text{targs}}})$, where the ith target is represented by χ_k^i. The track-state is $\xi_k = (\xi_k^1, \xi_k^2, ..., \xi_k^{N_{\text{targs}}})$ and $\mathbf{P}_k = (\mathbf{P}_k^1, ..., \mathbf{P}_k^{N_{\text{targs}}})$, where $(\xi_k^i, \mathbf{P}_k^i)$ is the ith target track-state. We use a zero-mean noise linearized target motion model for the target-state dynamics, given by $(\forall i)$

$$\chi^i_{k+1} = \mathbf{F}_k \chi^i_k + \nu^i_k, \qquad \nu^i_k \sim N(0, \mathbf{Q}_k) \tag{2}$$

with observations as defined in (1). The measurement error is $w^i_k \sim N(0, \mathbf{R}_k(\chi^i_k, s_k))$, and the target motion model (for all targets) is $\mathbf{F}_k$. The ith target state (χ^i_k) includes position coordinates (x_k, y_k), velocities (v^x_k, v^y_k), and accelerations (a^x_k, a^y_k) in x- and y-directions, i.e., $\chi^i_k = [x_k, y_k, v^x_k, v^y_k, a^x_k, a^y_k]^T$. The observation model becomes $\mathbf{H}_k = [\mathbf{I}_{2x2}, \mathbf{0}_{4x4}]$. A constant velocity (CV) model [7], [8] is implemented for target dynamics in (2), which defines $\mathbf{F}_k$. The ith target belief state, with assumed Gaussian distributions, can be expressed as $b^{\chi^i}_k(\chi) = N(\chi - \xi^i_k, \mathbf{P}^i_k)$, where ξ^i_k and $\mathbf{P}^i_k$ are the ith target track-states, which evolve according to the JPDA algorithm [7], [9].

The objective function is approximated by the NBO method as $J_H(b_0) \approx \sum_{k=0}^{H-1} c(\hat{b}_k, u_k)$, where $\hat{b}_1, \hat{b}_2, ..., \hat{b}_{H-1}$ is a nominal belief-state sequence over an optimized action sequence $u_0, u_1, ..., u_{H-1}$. The ith target nominal belief-state sequence, developed from nominal tracks $(\hat{\xi}^i_k, \hat{\mathbf{P}}^i_k)$ using a zero-noise Kalman filter [7], [8] is: $\hat{b}^{\chi^i}_k(\chi) = N(\chi - \hat{\xi}^i_k, \hat{\mathbf{P}}^i_k)$, where $\hat{\xi}^i_{k+1} = \mathbf{F}_k \hat{\xi}^i_k$, and

$$\hat{\mathbf{P}}^i_{k+1} = \begin{cases} [[\hat{\mathbf{P}}^i_{k+1|k}]^{-1} + \mathbf{S}^i_{k+1}]^{-1} & \text{if measurement available} \\ \hat{\mathbf{P}}^i_{k+1|k} & \text{otherwise} \end{cases} \tag{3}$$

where $\hat{\mathbf{P}}^i_{k+1|k} = \mathbf{F}_k \hat{\mathbf{P}}^i_k \mathbf{F}^T_k + \mathbf{Q}_k, \mathbf{S}^i_{k+1} = \mathbf{H}^T_{k+1}[\mathbf{R}_{k+1}(\hat{\xi}^i_{k+1}, s_{k+1})]^{-1}\mathbf{H}_{k+1}$ and $s_{k+1} = \Psi(s_k, u_k)$ (Ψ is defined in the next subsection). The nominal error covariance matrix $\hat{\mathbf{P}}^i_{k+1}$ in (3) is dependent upon the availability of future observations. Because of the uncertainty of future observations we can check for target observability by guessing the target location at time $k+1$ as $\hat{\xi}^{i,pos}_{k+1}$ and checking its line of sight from the sensor location (s^{pos}_{k+1}), where $\hat{\xi}^{i,pos}_{k+1}$ is the ith target nominal track-state at time $k+1$. We can write the cost function, defined as the mean-squared error between the targets and the tracks, as: $c(\hat{b}_k, u_k) = \sum_{i=1}^{N_{\text{targs}}} \text{Tr}\hat{\mathbf{P}}^i_{k+1}$. We want to find the sequence of actions $(u_0, u_1, ..., u_{H-1})$ that minimizes the cumulative cost function (truncated horizon [5]) $J_H(b_0) = \sum_{k=0}^{H-1} \sum_{i=1}^{N_{\text{targs}}} \text{Tr}\hat{\mathbf{P}}^i_{k+1}$, where $\hat{\mathbf{P}}^i_{k+1}$ represents the ith targets nominal error covariance matrix at time $k+1$. A "receding horizon control" approach is adopted, which optimizes the action sequence for $\mathbf{H}$ time-steps from the current time-step but only the action corresponding to the current time-step is implemented. At the next time-step, we perform a new action sequence optimization for $\mathbf{H}$ time-steps.

The measurement error, w_k in (1), is normally distributed $N(0, \mathbf{R}_k(\chi_k, s_k))$, where $\mathbf{R}_k$ contains q-rad angular uncertainty and $p\%$ range uncertainty. If the distance between the sensor and the target at time k is r_k, then the standard deviations corresponding to the range ($\sigma_{\text{range}}(k)$) and the angle ($\sigma_{\text{angle}}(k)$) are $\sigma_{\text{range}}(k) = (p/100)r_k$ and $\sigma_{\text{angle}}(k) = qr_k$. The information matrix depends on the inverse of the measurement covariance matrix, which depends on the distance between the sensor and the target. Therefore, the information matrix blows up when the UAV is exactly on top of the target (i.e., when $r_k = 0$ the sensor's location overlaps with the target's location in our 2-D environment). To address this problem, we define the effective distance (r_{eff}) between the sensor and the target as follows: $r_{\text{eff}}(k) = \sqrt{r_k^2 + b^2}$, where r_k is the actual distance between the target and the sensor and b is some non-zero real value. Therefore, the standard deviations of the range and the angle are given by $\sigma_{\text{range}}(k) = (p/100)r_{\text{eff}}(k)$ and $\sigma_{\text{angle}}(k) = qr_{\text{eff}}(k)$. If α_k is the angle between the target and the sensor at time k, then $\mathbf{R}_k$ is calculated as follows:

$$\mathbf{R}_k = \mathbf{M}_k \begin{bmatrix} \sigma^2_{\text{range}}(k) & 0 \\ 0 & \sigma^2_{\text{angle}}(k) \end{bmatrix} \mathbf{M}^T_k \qquad \text{where}$$

$$\mathbf{M}_k = \begin{bmatrix} \cos(\alpha_k) & -\sin(\alpha_k) \\ \sin(\alpha_k) & \cos(\alpha_k) \end{bmatrix}.$$

The eigenvalues of the matrix $\mathbf{R}_k$ are therefore $\sigma^2_{\text{range}}(k)$ and $\sigma^2_{\text{angle}}(k)$.

IV. UAV KINEMATICS AND FIXED FOV

Simplified UAV kinematics are used for calculating the UAV motion. Using a fixed FOV sensor, the FOV can be calculated in camera axes. Using Euler angle transformations, we can determined if the target is within the sensor FOV.

A. UAV Kinematics

In this subsection we define the mapping function Ψ introduced in Section III to describe the evolution of the sensor (UAV) state given an action, i.e., $s_{k+1} = \Psi(s_k, u_k)$. The state of the ith UAV at time k is given by $s^i_k = (p^i_k, q^i_k, V^i_k, \theta^i_k)$, where (p^i_k, q^i_k) represents the position coordinates, V^i_k represents the speed, and θ^i_k represents the heading angle. Let a^i_k be the forward acceleration (control variable) and ϕ^i_k be the bank angle (control variable) of the UAV, i.e., $u^i_k = (a^i_k, \phi^i_k)$. The mapping function Ψ can be specified as a collection of simple kinematic equations that govern the UAV motion. The kinematic equations of the UAV motion are as follows. The speed is updated according to $V^i_{k+1} = [V^i_k + a^i_k T]^{V_{\max}}_{V_{\min}}$, where $[v]^{V_{\max}}_{V_{\min}} = \max\{V_{\min}, \min(V_{\max}, v)\}$, where $V_{\min}$ and $V_{\max}$ are the minimum and the maximum limits on the speed of the UAVs. The heading angle is updated according to $\theta^i_{k+1} = \theta^i_k + (gT\tan(\phi^i_k)/V^i_k)$, where g is the acceleration due to gravity and T is the length of the time-step. The position coordinate are updated according to $p^i_{k+1} = p^i_k + V^i_k T\cos(\theta^i_k)$ and $q^i_{k+1} = q^i_k + V^i_k T\sin(\theta^i_k)$.

B. Fixed FOV Calculation

Given a sensor width (x_{sens}) and height (y_{sens}), along with the focal length (f) of an installed sensor, a FOV can be calculated for a given altitude (z). The angular FOV for the sensor width is $\text{FOV}_w = 2\tan^{-1}(x_{\text{sens}}/2f)$ and for the sensor height is $\text{FOV}_h = 2\tan^{-1}(y_{\text{sens}}/2f)$. Given a height above the ground, the edges of the FOV can be calculated in camera

axes. We assume that the camera is installed concurrent to the body axis, for ease of calculation. The top and bottom edges of the FOV are $x_{FOV} = \pm \text{z} \tan(0.5\text{FOV}_h)$ and the left and right edges of the FOV are $y_{FOV} = \pm \text{z} \tan(0.5\text{FOV}_w)$, where z is the altitude of the sensor.

To determine if an observation is made, the position of the target must be translated and rotated into the UAV body axis. A vector η is calculated between the UAV position and the target position as $\eta = (p_{\text{UAV}} - p_{\text{target}}, q_{\text{UAV}} - q_{\text{target}}, \text{z}_{\text{UAV}} - \text{z}_{\text{target}})$. Given the UAV Euler angles, pitch (θ_{UAV}), roll (ψ_{UAV}), and heading (ϕ_{UAV}) a rotation of η can be made between the world axis and body axis. The value of η in the body axis can now be compared to the FOV for the sensor. If the position of the target, η, is within the field of view, an observation is made and the tracker will update normally with an updated observation, as specified in (1). However, if η is not in the FOV, there will be no observation and no measurement will be passed to the tracker.

V. FUEL BURN COST FUNCTION

The nominal cost function often used for vehicle control is focused purely on the estimated target location error, based on the trace of the covariance $\mathbf{P}_k$. This simple cost function results in significant dynamics of the UAV to try to precisely track the target for as accurate of a target location estimate as possible. However, as a result, the increased dynamics results in less endurance. There are times during missions that maintaining observations of the target is important, but the accuracy of the estimated location is less of a concern. In these cases, increasing the mission endurance of the UAV by decreasing the dynamics becomes a viable option.

Depending on the level of desired tracking accuracy versus the increased mission endurance, the cost function can be updated to include a fuel burn estimate. A fuel-burn $\mathbf{B}$ can be included in the cost function, with a set of ratio variables, λ_1 and λ_2, to vary the impact of the error compared to the fuel burn by:

$$J_H(b_0) = \sum_{k=0}^{H-1} (\sum_{i=1}^{N_{\text{targs}}} \lambda_1 \text{Tr}\hat{\mathbf{P}}^i_{k+1}) + \lambda_2 \mathbf{B} \tag{4}$$

The trace of the estimated covariance is calculated for all targets across the horizon of concern and the fuel burn is calculated by estimating the power usage of the UAV during the horizon. The burn value used will be based upon the specific vehicle implemented on.

VI. WEIGHTED TRACE PENALTY

When using a limited FOV sensor there are conditions when the UAV may not be able to observe the target for an extended period of time. As a result, the POMDP algorithm may be unable to determine an adequate path plan, due to extended non-observation across the limited horizon. This can be exacerbated when trying to limit maneuvering for fuel efficiency. To determine a sufficient path we incorporate a *Weighted Trace Penalty (WTP)* term into the calculation of the next best UAV command. The WTP term was previously developed as an estimated cost to go (ECTG) term to deal with occlusions preventing observations [5]. We can estimate this growth with a WTP term, which is a product of the current covariance trace and the minimum distance to observability (MDO) for the non-observed target. The terminal cost or ECTG term using the WTP takes the form:

$$\hat{J}(b) = J_{\text{WTP}}(b) := \gamma D(s, \xi^q) \text{Tr} P^q \tag{5}$$

where γ is a positive constant, q is the index of the worst non-observed target. The MDO, $D(s, \xi)$, is the distance from the UAV to the closest point where the target becomes observable. The addition of the WTP results in a final cost function, which is used for the experimentation, of:

$$J_H(b_0) = \sum_{k=0}^{H-1} (\sum_{i=1}^{N_{\text{targs}}} \lambda_1 \text{Tr}\hat{\mathbf{P}}^i_{k+1}) + \lambda_2 \mathbf{B} + \gamma D(s, \xi^{\boldsymbol{q}}) \text{Tr}\mathbf{P}^q \tag{6}$$

VII. EXPERIMENTS

Statistical analysis, based upon 500 Monte Carlo simulations per configuration, was performed to evaluate the effectiveness of our method to track the target with varying fuel efficiency. The number of targets tracked, the altitude of the UAV, and the burn ratio of the cost function were all varied for the experiment. The cost function defined in equation 6 was utilized with a γ of 250 is used. A single UAV tracked either one or two targets. Previous research with a fixed FOV sensor configuration has shown that above 1000 meters the impact of the sensor FOV is minimal. Therefore, only three altitudes were evaluated: 200, 500, and 1000 meters. A burn ratio (tracking accuracy:fuel burn, $\lambda_1 : \lambda_2$) of 1:0, 1:1, 1:5, 1:10, and 1:15 were used for single and two target tracking. Additionally, a burn ration of 1:20 was also performed for single target to evaluate whether the burn savings had reached a minimum yet. A range uncertainty of 10 percent and an angular uncertainty of 1 percent were used for this evaluation. The sensor was fixed in a 90 degree straight down FOV configuration, relative to the UAVs nose. A horizon window of 6 steps, at 2 seconds per step, was used for the trajectory calculation. The trajectory calculation was performed every 4 seconds. A 400 second duration was used for each Monte Carlo simulation.

The sensor simulated was modeled after several commercially available sensors [20]. The sensor was assumed to have a focal plane width of 5 mm, height of 3 mm, and a lens focal length of 5.3 mm. This configuration provides a field of view of 50.5 degree wide and 31.6 degrees tall. It is assumed at the altitudes tested, the sensor is capable of resolving the target sufficiently for tracking.

The targets moved at a constant speed of 10 m/s at a constant heading (unknown to the tracker). The UAV was allowed to vary speed between 16 and 25 m/s and a maximum bank angle of 30 degrees. To provide a consistent analysis baseline, altitude was only considered for variation of sensor field of view; otherwise the problem was treated as a 2-D problem. Tracking errors were not considered as a function of altitude, only of x-y distance variations to enable FOV comparison. Previous efforts have shown that the

average location error was 2-3 meters for single target and 5-6 meters for multiple target tracking in similar scenarios [2].

A basic fuel-burn calculation based upon actual power usage of a small UAV was used [21]. Measurements of real-time energy usage (in watt-hr) from a fixed-speed commercially available small UAV were taken while the vehicle was flying constant altitude and either wings level or in a full bank. Data showed that the power usage between wings level and full bank were essentially linear. For simplicity, it is assumed that the aircraft is symmetric such that left or right bank angle require the same energy. The burn was estimated across the speed range to extend from just a fixed speed aircraft. Table I provides simple lookup values for interpolating fuel burn.

TABLE I
FUEL BURN VALUES

Velocity (m/s)	Wings Level (Watt-hr)	30 deg Bank (Watt-hr)
14	95	110
20	105	120
25	112	135
30	119	145
35	130	160

A. Results

Overall, the algorithm showed reasonable ability to track moving targets while providing fuel-efficient options. As previously seen, at lower altitudes, the tracking errors are generally higher due to reduced observations. The modified cost function provided the ability to increase endurance by 6-9% while still providing tracking ability. The increase in tracking errors due to the change in fuel burn were still reasonable for general tracking of a moving target that doesn't require high quality accuracy.

Based on the fuel usage model of the UAV, if the vehicle were to fly straight and level (most efficient possible) at a speed of 14 m/s for a 400 second window, the UAV would use 10.56 W, or 95 W for an hour. At 35 m/s, that would result in 14.4 W for 400 seconds, or 130 W for an hour. However, because the vehicle must maneuver, an increase in power usage is experienced.

The average tracking errors and fuel burn were calculated for each altitude and burn ratio configuration. Figure 1 provides the comparison of mean tracking error and mean fuel burn for a 400 second simulation for a single target. Figure 2 shows the mean percent of observations for each configuration compared to the mean location error. The symbols indicate which burn ratio was used, and the line connected to the given symbol indicate the altitude for the simulation. The trace:burn ratio provides the values of $\lambda_1 : \lambda_2$. As can be seen, as the fuel-burn ratio is increased, the fuel consumption is reduced while the tracking error is increased. As can be seen at all three altitudes, the fuel-burn ratio reduces the overall fuel use while showing an increase in tracking errors, as expected.

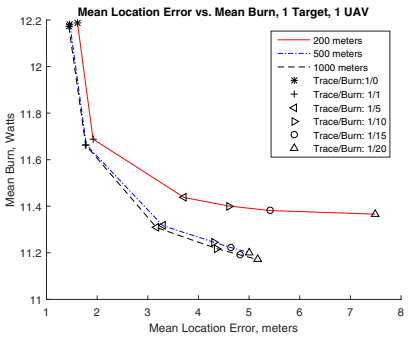

Fig. 1. Average Location Error vs Fuel Burn, 1 UAV, 1 Target

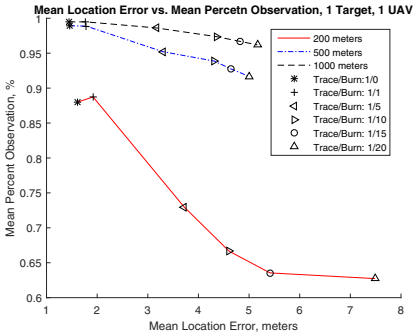

Fig. 2. Average Location Error vs. Percent Observation, 1 UAV, 1 Target

Figure 3 shows the mean tracking error versus mean fuel burn for two target tracking. Figure 4 shows the mean percent observations versus mean tracking error. The mean location errors and mean observation percentages are the average of all 500 runs for both targets. Only 500 and 1000 meter configurations are shown as the 200 meter data showed inadequate performance of tracking the second target. Over half of the runs at 200 meters indicated the UAV never made an observation of the second target. As can be seen, an increase in tracking error, corresponding to reduced observations, can be seen as we increase the fuel burn. At 1000 meters it can be noted that the change in fuel burn has a minimal impact on mean tracking errors.

While the 500 and 1000 meter tracking showed good performance, the 200 meter errors with two targets was

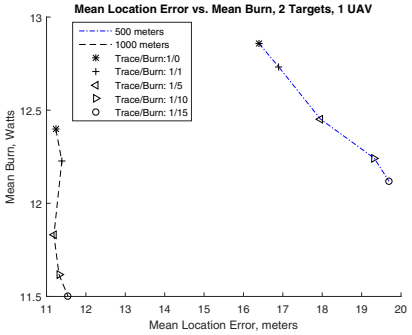

Fig. 3. Average Location Error vs Fuel Burn, 1 UAV, 2 Targets

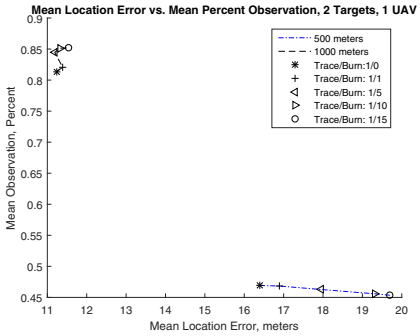

Fig. 4. Average Location Error vs. Percent Observation, 1 UAV, 2 Targets

TABLE II
MEAN FUEL BURN, 1 TARGET

$Ratio$	200 m	500 m	1000 m
$1:0$	12.19	12.18	12.17
$1:20$	11.37	11.2	11.17
$\%gain$	7.2%	8.75%	8.95%

inadequate. One source of the poor performance is due to the MATLAB fmincon optimization function finding a local minimum and not the global minimum. This generally forces the UAV to stay closer to the first target. Additional minimization options and heuristics will be investigated for future development. Finally, due to the limited FOV of the sensor, the best way to improve the performance would be to either incorporate a sensor with a larger FOV or incorporate a gimbaled control of the sensor.

As discussed earlier, the fuel burn flying a pure straight and level 400 second flight would be 10.56 W. Tables II and III show the burns for single and two target tracking for each burn configuration. As can be seen, for single target tracking, an approximately 7-9% increase in fuel efficiency is noted from the 1:0 configuration as compared to the 1:20 configuration. As the altitude increases, the savings increase due to the increased sensor footprint allows reduced maneuvering while still gaining observations. For two target tracking, an approximately 6-8% increase in fuel efficiency is noted from the 1:0 configuration as compared to the 1:15 configuration. As with single target, increased altitude increases the fuel burn due to sensor footprint.

VIII. CONCLUSIONS

The fuel efficient POMDP presented provides a robust tracking solution that enables fuel efficient options. Highly accurate tracking with a limited FOV sensor flying at low altitude is a difficult use case for UAVs. Significant maneuvering is required for a UAV to provide high quality tracking with minimal errors but leads to reduced endurance. Using a fuel-burn component in the cost function of the POMDP, alongside a Weighted Trace Penalty provides a highly capable tracker with improved endurance opportunities. Endurance increases of 6-9% were experienced while still providing useful tracks of moving targets. Improvements in lower-altitude tracking of multiple targets may be seen by incorporating a gimbaled sensor.

TABLE III
MEAN FUEL BURN, 2 TARGETS

$Ratio$	500 m	1000 m
$1:0$	$12.86W$	$12.40W$
$1:15$	$12.12W$	$11.5W$
$\%gain$	6.1%	7.8%

REFERENCES

[1] C. M. Eaton, E. K. P. Chong, and A. A. Maciejewski, "Multiple-Scenario Unmanned Aerial System Control: A Systems Engineering Approach and Review of Existing Control Methods," *Aerospace*, vol. 3, no. 1, pp. 1–26, Jan. 2016.

[2] C. M. Eaton, E. K. P. Chong, and A. A. Maciejewski, "Robust UAV Path Planning using POMDP with Limited FOV Sensor," in *Proc. 2017 IEEE Conf. Control Technology and Application,* Kohala Coast, HI, USA, Aug 2017, pp 1530–1535.

[3] S. Ragi and E. K. P. Chong, "UAV Guidance Algorithms Via Partially Observable Markov Decision Processes," in *Handbook of Unmanned Aerial Vehicles*, K.P. Valavanis, G.J. Vachtsevanos, Eds., Netherlands: Springer, 2015, pp. 1775–1810.

[4] S. Ragi and E. K. P. Chong,"UAV path planning in a dynamic environment via partially observable Markov decision process," *IEEE Trans. Aerosp. Electron. Syst.*, vol. 49, no. 4, pp. 2397–2412, Oct. 2013.

[5] S. A. Miller, Z. A. Harris, and E. K. P. Chong, "A POMDP framework for coordinated guidance of autonomous UAVs for multitarget tracking," *EURASIP J. Adv. Signal Process.*, vol. 2009, 2009.

[6] L. W. Krakow and E. K. P. Chong, "Autonomous UAV Control: Balancing Target Tracking and Persistent Surveillance," in *Proc. 2017 IEEE Conf. Control Technology and Application,* Kohala Coast, HI, USA, Aug 2017, pp 1524–1529.

[7] S. Blackman and R. Popoli, *Design and Analysis of Modern Tracking Systems*. Norwood, MA: Artech House, 1999.

[8] Y. Bar-Shalom, X. R. Li, and T. Kirubarajan, *Estimation with Applications to Tracking and Navigation*. Hoboken, NJ: Wiley-Interscience, 2001.

[9] Y. Bar-Shalom and T. E. Fortmann, *Tracking and Data Association*. Waltham, MA: Academic Press, 1988.

[10] E. K. P. Chong, C. Kreucher, and A. O. Hero III, "Partially observable Markov decision process approximations for adaptive sensing," *Discrete Event Dynamic Systems*, vol. 19, 2009, pp. 377–422.

[11] R. Bellman, *Dynamic Programming*. Princeton, NJ: Princeton University Press, 1957.

[12] C. Kreucher, A. O. Hero III, K. Kastella, and D. Chang, "Efficient methods of non-myopic sensor management for multitarget tracking." in *Proc. 43rd IEEE Conf. Decision and Control*, Paradise Island, Bahamas, Dec. 2004, pp. 722–727.

[13] D. P. Bertsekas and J. N. Tsitsiklis, *Neuro-Dynamic Programming*. Belmont, MA: Athena Scientific, 1996.

[14] R. S. Sutton and A. G. Barto, *Reinforcement Learning: An Introduction*. Cambridge, MA: MIT Press, 1998.

[15] D. P. Bertsekas and D. A. Castanon, "Rollout algorithms for stochastic scheduling problems." *J. Heuristics*, vol. 5, no. 1, Apr. 1999, pp. 89–108.

[16] E. K. P. Chong *et al.*, "A framework for simulation-based network control via hindsight optimization," *Proc. 39th IEEE Conf. Decision and Control*, Sydney, Australia, Dec. 2000, pp. 1433–1438.

[17] G. Wu *et al.*, "Burst-level congestion control using hindsight optimization," *IEEE Trans. Autom. Control*, vol. 47, no. 6, 2002, pp. 979–991.

[18] D.P. Bertsekas, *Dynamic Programming and Optimal Control (vol. 2)*, Belmont, MA: Athena Scientific, 2007.

[19] D.P. Bertsekas, "Dynamic programming and suboptimal control: A survey from ADP to MPC," *European J. on Control: Fundamental Issues on Control*, vol. 11, pp. 4–5, 2005.

[20] Sony FCBEV7500 Camera Block, https://pro.sony.com/bbsc/ssr/cat-camerasindustrial/cat-ciblockcameras/product-FCBEV7500/ accessed Mar. 2017.

[21] BirdsEyeView Aerobatics FireFLY6 Pro, https://www.birdseyeview.aero/ accessed Jan. 2018.